Materials Research. 2010; 13(4): 457-464

Workability Studies on Cold Upsetting of Sintered Copper Alloy Preforms

Ananthanarayanan Rajeshkannan*

Division of Mechanical Engineering, School of Engineering and Physics,
Faculty of Science, Technology and Environment, The University of the South Pacific,
Laucala Campus, Suva, Fiji

Received: June 1, 2010; Revised: November 17, 2010

The major concern of the design for manufacturability is to accomplish the require deformation without failure of work material. The degree of deformation that can be achieved in a particular metal forming process without creating condition is termed as workability. The present investigation pertains to study the cold workability behaviour of Cu-7%Al-1.8%Si sintered preforms. Cold upsetting of these preforms with various aspect ratios were carried out and the working behaviour of the preforms at various stress state conditions was computed. The analysis measured for different components such as stress formability index and obtained density during secondary deformation as a function of induced strain. Similarly various computed stress ratio parameters with induced strain.

Keywords: *workability, stress formability index, stresses, strains*

1. Introduction

Workability of fully dense materials indicates that careful control of the deformation can reduce or eliminate the local stress and strain states that lead to fracture. The exhaustion of workability manifests itself as ductile fracture during metal working processes. The prediction of fracture in the design stage accordingly its early modification promotes economically viable. Ductile fracture in metal working has been modeled in several ways, based on the different concepts on the initiation of fracture in a plastically deforming material. Saanouni[1] proposed a numeric model to predict the ductile fracture initiation and growth during metal forming process, further its capability is tested by various 2D and 3D samples. It has been predicted[2] that cumulative specific plastic energy adjusted suitably with the ultimate tensile stress are the most reliable factor in determining the workability limits which has been evaluated through comparative evaluation of various theoretical failure criteria. Landre et al.[3] were reported that the ductile fracture criteria in conjunction with finite element method can be used to predict the materials likely initiation to fracture during cold forging. Petruska and Janicek[4] studied the fracture of cylindrical specimen with longitudinal surface notch compression test, which evaluates the ability of various ductile fracture criteria of different geometry and end conditions to predict the failure initiation. Abdel-Rahman and El-Sheikh[5] investigated the effect of relative density on the forming limits of sintered preforms while upsetting, also presented effect of various stresses as a function of relative density. In fact many investigators[6-8] made an attempt to explain ductile fracture in terms of void initiation, growth and finally coalescence to eventually result in to fracture. Vujovic and Shabaik[9] modeled fractures in metal working in consideration of stress formability index and strain to fracture. A computer aided evaluation system, coupled with elasto-plastic large strain finite element package to check for ductile fracture in bulk forming processes was developed using different workability criteria[10].

A generalized yield criterion and some plastic constitutive equations for sintered powder materials were developed by Lin et al.[11]. This yield criterion can depict both initial and successive yield in the form of unified yield function, which comprehensively establish the effect of initial density and strengthening characteristics. Pokorska[12] determined the apparent yield stress for P/M materials by considering three kinds of materials include iron, copper and aluminum. The deformability of sintered materials was evaluated[13] on the basis of the limiting plasticity diagrams, characterizing the variation of the strain of the material to fracture in relation to the parameter of the stress state. Aubertin and Li[14] proposed a multi-axial yield criterion that can be applicable to variety of materials and loading state, its main advantage is explicitly porosity dependent. A plasticity criterion is proposed[15] for powdered materials which account the local character of slip and plastic deformation of the particles; further it presented a method of finding the empirical parameters on the plasticity criterion. A new algorithm been developed[16] and is successfully implemented into general purpose finite element program to study and yield a flexible solution for different yielding criterion for sintered porous materials. A similar analysis but some more published elasto-plastic models is considered in the created constitutive model and the same has been reported[17], which in general ensure that porous materials can also be studied in general purpose finite element program.

In this paper, a complete investigation on the workability criteria of sintered Cu-7%Al-1.8%Si powder preforms was made. P/M preforms with various aspect ratios were discussed to explore the forming behavior during cold upsetting under various triaxial stress state conditions. Computation methods for determining various stress ratios involved in workability behavior were also presented.

2. Theoretical Analysis

The various upsetting parameters that influence workability characteristics of the selected alloy under various stress state conditions been developed, following are the respective discussions.

2.1. Uniaxial stress state condition

In the upsetting of a porous preform, under frictional conditions, the average density is increased. It has been established that friction promotes densification at the same time reduces the height strain to

*e-mail: rkanitt@gmail.com

fracture. The state of stress in a homogeneous compression process is as follows: According to Abdel-Rahman and El-Sheikh[5]:

$$\sigma_z = -\sigma_{eff},\ \sigma_r = \sigma_\theta = 0 \tag{1}$$

$$\sigma_m = (\sigma_z / 3) = -(\sigma_{eff} / 3) \tag{2}$$

and the strain state is:

$$\varepsilon_z = -\varepsilon_{eff} = \ln\left(H_f / H_0\right) \tag{3}$$

and

$$\varepsilon_\theta = \varepsilon_r = \ln\left(D_f / D_0\right) \tag{4}$$

As, compression continues, the final diameter increases and the corresponding hoop strain that is tensile in nature, also increases until it reaches the fracture limit. Once the fracture is initiated, the forming limit strain is the same as the effective strain and is determined from:

$$\varphi_{eff} = \ln\left(H_0 / H_f\right) \tag{5}$$

As an evidence of experimental investigation implying the importance of the spherical component of the stress state on fracture, Vujovic ad Shabaik[9] proposed an expression for the stress formability index β, which determines the fracture limit and is given by

$$\beta = \left(3\sigma_m / \sigma_{eff}\right) \tag{6}$$

2.2. Plane stress state condition

The state of stress in a plane stress condition ($\sigma_r = 0$), associated to flow characteristics of porous materials has been expressed elsewhere[18], which is given by:

$$\frac{d\varepsilon_\theta}{d\varepsilon_z} = \left(\frac{\sigma_\theta - \gamma\sigma_z}{\sigma_z - \gamma\sigma_\theta}\right) \tag{7}$$

where, $\gamma = (\varepsilon_\theta / 2\varepsilon_z)$

Equation 7 can be further simplified as follows:

$$\frac{\sigma_\theta}{\sigma_z} = \left(\frac{\alpha + \gamma}{1 + \alpha\gamma}\right) \tag{8}$$

where, $\alpha = (d\varepsilon_\theta / d\varepsilon_z)$

The hoop strain, ε_θ of the compact is determined as explained elsewhere[18], which includes the bulge diameter and contact diameter and Equation 3 follows for ε_z:

$$\varepsilon_\theta = \ln\left(\frac{2D_b^2 + D_c^2}{3D_0^2}\right) \tag{9}$$

For Plane stress state condition, σ_m follows:

$$\sigma_m = \frac{\sigma_\theta + \sigma_z}{3} \tag{10}$$

Equation 10 can be rearranged as:

$$\frac{\sigma_m}{\sigma_z} = \frac{1}{3}\left(1 + \frac{\sigma_\theta}{\sigma_z}\right) \tag{11}$$

From[21], the relationship between σ_{eff} and σ_z can be written as follows:

$$\sigma_{eff} = (0.5 + \alpha)\left[3\left(1 + \alpha + \alpha^2\right)\right]^{0.5}\sigma_z \tag{12}$$

Equation 12 is rearranged as:

$$\frac{\sigma_{eff}}{\sigma_z} = (0.5 + \alpha)\left[3\left(1 + \alpha + \alpha^2\right)\right]^{0.5} \tag{13}$$

The β provided in the Equation 6 can be derived for the biaxial stress state condition from Equations 11 and 13 as follows:

$$\beta = 3\left(\frac{\left[\sigma_m / \sigma_z\right]}{\left[1 / \left(\sigma_{eff} / \sigma_z\right)\right]}\right) \tag{14}$$

2.3. Triaxial stress state condition

The state of stress for triaxial condition is given below, as explained elsewhere[19]

$$\alpha = \frac{d\varepsilon_\theta}{d\varepsilon_z} = \frac{A\sigma_\theta - R^2 B}{A\sigma_z - R^2 B} \tag{15}$$

where, $A = (2 + R^2)$; $B = (\sigma_z + 2\sigma_\theta)$ and $R = (\rho_f / \rho_{th})$.

From Equation 15, σ_θ can be determined as given below:

$$\sigma_\theta = \sigma_z\left[\frac{2\alpha + R^2}{2 - R^2 + 2R^2\alpha}\right] \tag{16}$$

Further rearranging Equation 16 solves into the form as given below:

$$\frac{\sigma_\theta}{\sigma_z} = \left[\frac{2\alpha + R^2}{2 - R^2 + 2R^2\alpha}\right] \tag{17}$$

For triaxial state of cylindrical coordinates, σ_m can be written as follows:

$$\sigma_m = \frac{\sigma_z + \sigma_r + \sigma_\theta}{3} \tag{18}$$

It is assumed that $\sigma_r = \sigma_\theta$, for the case of axisymmetric condition, substituting this expression in Equation 18 and further rearranging deduced as follows:

$$\frac{\sigma_m}{\sigma_z} = \frac{1}{3}\left[1 + \frac{2\sigma_\theta}{\sigma_z}\right] \tag{19}$$

The effective stress can be determined from the following expression as explained elsewhere[20].

$$\sigma_1^2 + \sigma_2^2 + \sigma_3^2 - R^2\left(\sigma_1\sigma_2 + \sigma_2\sigma_3 + \sigma_3\sigma_1\right) = \sigma_{eff}^2\left(2R^2 - 1\right) \tag{20}$$

This expression can be written for cylindrical coordinates as follows:

$$\sigma_z^2 + \sigma_r^2 + \sigma_\theta^2 - R^2\left(\sigma_z\sigma_r + \sigma_r\sigma_\theta + \sigma_\theta\sigma_z\right) = \sigma_{eff}^2\left(2R^2 - 1\right) \tag{21}$$

As, $\sigma_r = \sigma_\theta$ for cylindrical axisymmetric upsetting, with further rearrangement the Equation 21 follows as:

$$\frac{\sigma_{eff}}{\sigma_z} = \left\{\frac{1 + 2\left(\sigma_\theta / \sigma_z\right)^2 - R^2\left[2\left(\sigma_\theta / \sigma_z\right) + \left(\sigma_\theta / \sigma_z\right)^2\right]}{2R^2 - 1}\right\}^{1/2} \tag{22}$$

The β provided in the Equation 6 can be derived for the triaxial stress state condition from Equations 19 and 22 as follows:

$$\beta = 3\left(\frac{\left[\sigma_m/\sigma_z\right]}{\left[1/\left(\sigma_{eff}/\sigma_z\right)\right]}\right) \quad (23)$$

3. Experimental Details

3.1. Materials and characteristics

Electrolytic copper powder of less than 150 μm was procured and analysed for its purity, which was found to be 99.7% and the rest were insoluble impurities. The atomized aluminium powder and silicon powder of less than 37 μm size were also analyzed for its purity, which were found to be 99.93 and 99.90% respectively. All the aforementioned powders were obtained from M/S. Metal Powder Company, Thirumangalam, Madurai, Tamil Nadu, India.

3.2. Powder blending and compaction

The required amount of powders corresponding to C64200 that is Cu-7%Al-1.8%Si were measured and blended in a pot mill along with porcelain balls of ratio 1:1 by weight for a period of 18 hours in order to obtain homogeneous mix. The powder blend was die compacted to yield preform of 26 mm diameter with 16 & 26 mm heights on a 0.6 MN hydraulic press using a suitable die set assembly. The initial preform densities were maintained in the range of 80 ± 1 percent theoretical by employing pressure in the range of 280 ± 10 MPa.

3.3. Ceramic coating, drying and sintering

These green compacts were thoroughly coated on all surfaces with indigenously developed ceramic coating[21] in order to protect them against oxidation during sintering. This coat was allowed to dry for a period of 10 hours under room temperature conditions. Further, the compacts were recoated in the direction 90° to the earlier one. This second coat was allowed to dry under aforesaid condition for a further period of 10 hours. These ceramic-coated compacts were dried at 300 °C for a period of 30 minutes in an alumina boat placed inside the electric muffle furnace. After the drying sequence was completed, the furnace temperature was raised to 810 ± 10 °C. At this temperature, the compacts were sintered for 100 minutes followed by furnace cooling.

3.4. Cold deformation and measurements

The sintered preforms were cleaned from the ceramic residue and machined to such a dimension to provide the preforms of initial heights to diameter ratio (aspect ratio) of 0.60 and 1. These preforms were compressed between flat dies in 60 t capacity hydraulic press at an incremental loading step of 0.02 MN. After each step of loading, measurements of height, diameters (contact and bulged) using digital vernier caliper and density by invoking Archmedian principle and examination of the barreled surface of cracks were made. The preforms were deformed under dry friction condition. The schematic view of before and after deformation of the preform is shown in Figure 1.

4. Results and Discussion

Figure 2(a-d) have been plotted for the variation of the stress formability index (β) determined under the triaxial stress state as a function of the induced axial strain (ε_z). The values for β and ε_z can be respectively calculated from Equations 23 and 3. For all the aspect ratio, the stress formability index increases with increasing value of the axial strain, which can be understood from Figure 2a

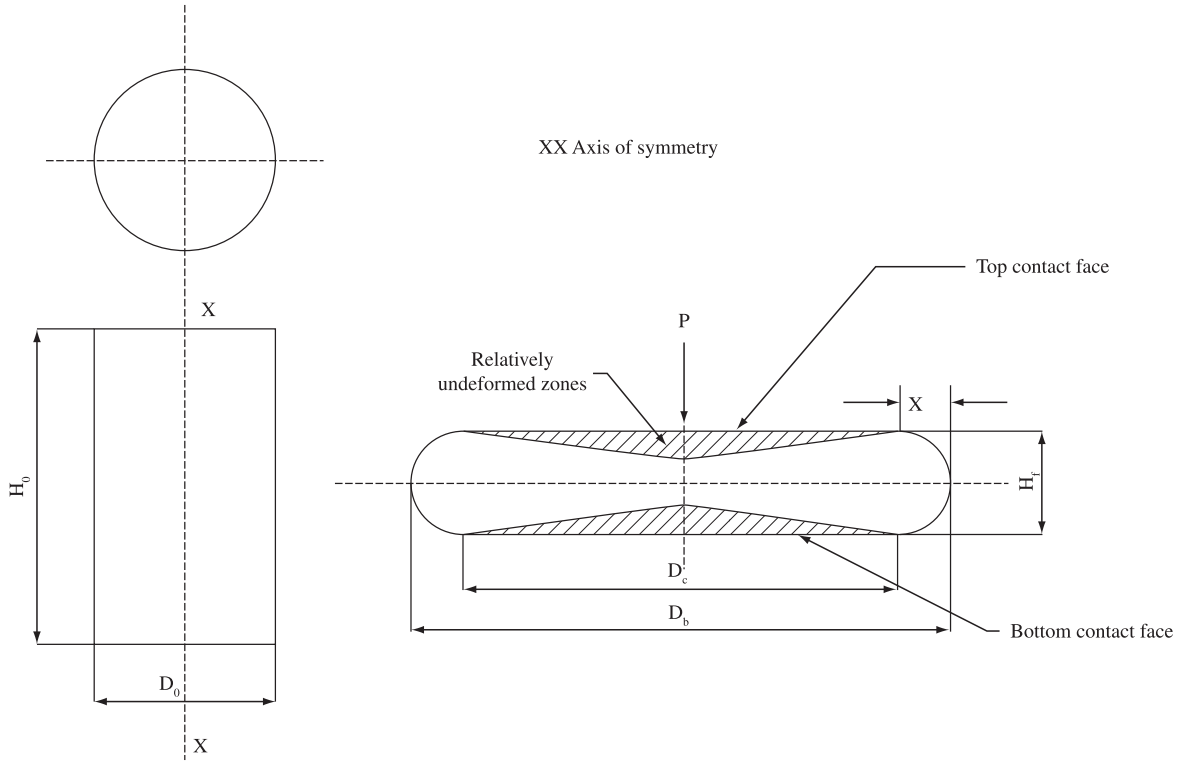

Figure 1. Schematic view of before and after deformation of the perform.

as it shows general characteristics where the lines drawn explicit two different stages respectively shown by dotted and continuous line for all the aspect ratios. Also, for any given axial strain, the stress formability index value found to be higher for smaller aspect ratio in comparing to its subsequent increment in aspect ratio of preforms. Particularly, this behaviour is more explicit, if axial strain value increases.

Curve fitting techniques applied for the plot between stress formability index and axial strain that includes linear curve, exponential curve and the polynomial curve of second order respectively shown in Figure 2b through d, the corresponding empirical relation and regression coefficient values are shown in Table 1. Although, it is observed that the correlation coefficient for all the obtained empirical relation is found to be near unity,

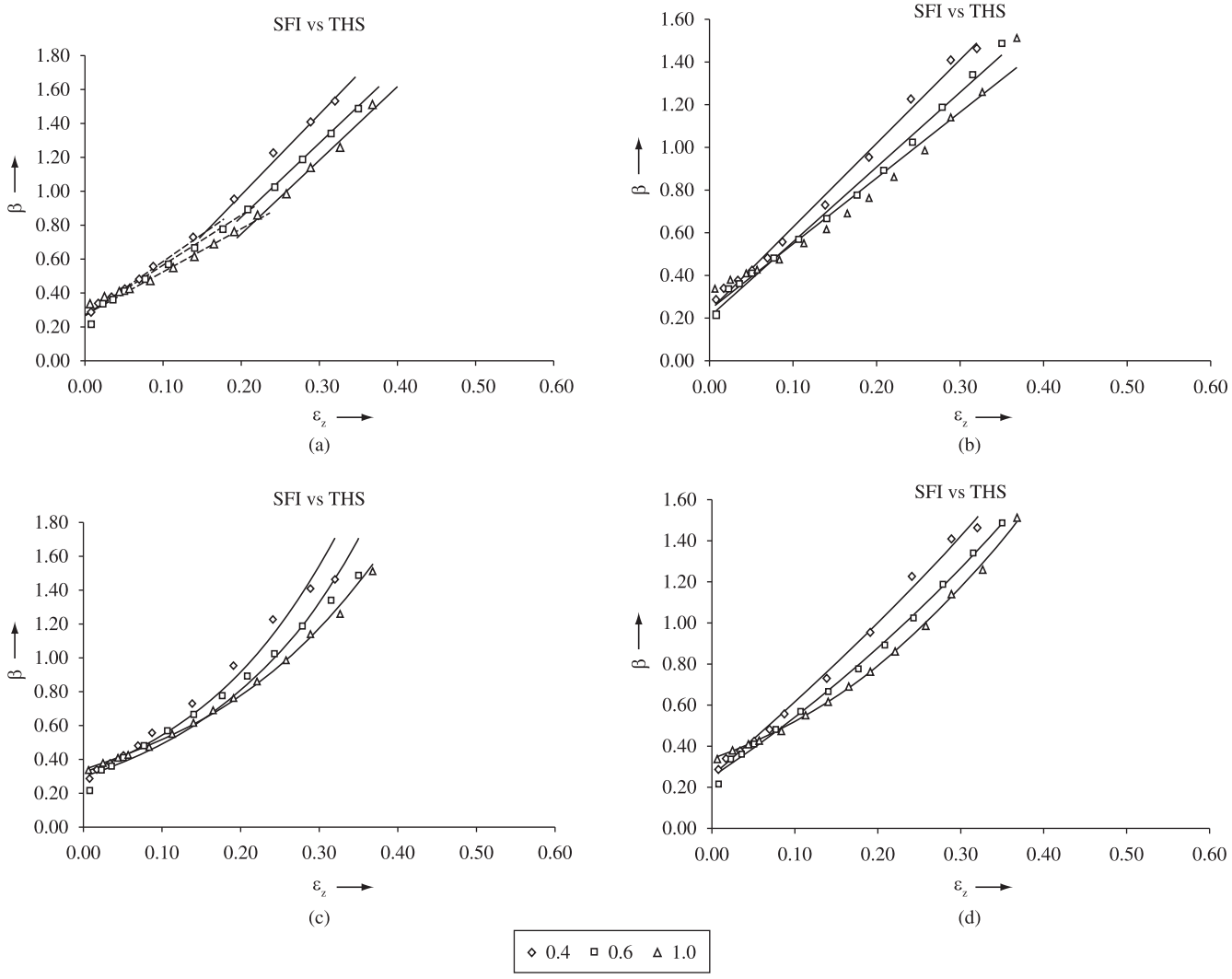

Figure 2. a) Relationship between β and ε_z; b) relationship between β and ε_z – linear curve fitting; c) relationship between β and ε_z – exponential curve fitting; and d) relationship between β and ε_z – parabolic curve fitting.

Table 1. Curve fitted results between β and ε_z.

Relationship	Aspect ratio	Name of the curve	Empirical equation	RC value
β vs. ε_z	0.40	Linear	$\beta = 3.9925\varepsilon_z + 0.2343$	0.9944
	0.60		$\beta = 3.5053\varepsilon_z + 0.2067$	0.9925
	1.0		$\beta = 3.0857\varepsilon_z + 0.2391$	0.9714
	0.40	Exponential	$\beta = 0.3227e^{5.207\varepsilon_z}$	0.9757
	0.60		$\beta = 0.2982e^{4.9716\varepsilon_z}$	0.9521
	1.0		$\beta = 0.3411e^{4.1093\varepsilon_z}$	0.9980
	0.40	Polynomial	$\beta = 1.6921\varepsilon_z^2 + 3.3841\varepsilon_z + 0.2565$	0.9955
	0.60		$\beta = 2.6974\varepsilon_z^2 + 2.5860\varepsilon_z + 0.2512$	0.9972
	1.0		$\beta = 5.1980\varepsilon_z^2 + 1.2139\varepsilon_z + 0.3408$	0.9987

polynomial expressions found to be the best for the selected range of the aspect ratios.

Further observed from polynomial expression that for nil value of strain, the value of stress formability index observed to be constant and its value is 0.3. In the same expression, its first order values found to decrease whilst the second order value increases with the increasing aspect ratio. This reveals that at initial stage, strain induced on the preform is profound that subsequently reflected in low variation of stress formability index, however decreasing aspect ratio enhances the stress formability index. This is due to the fact that the pore bed collapses at the earlier stages of deformation in lower aspect ratio preforms. The same reason holds for the later stages of deformation as well, when observing to the values of second order found to increase with the increasing aspect ratio that reveals the scope for strain inducement is relatively high when the aspect ratio is large, which subsequently decreases the stress formability index for larger aspect ratio preforms.

Figure 3(a-d) is drawn for relative density (R) to axial strain (ε_z) for the cold upsetting of Cu-7%Al-1.8%Si powder preform of various aspect ratios. The characteristic nature of these curves is similar for

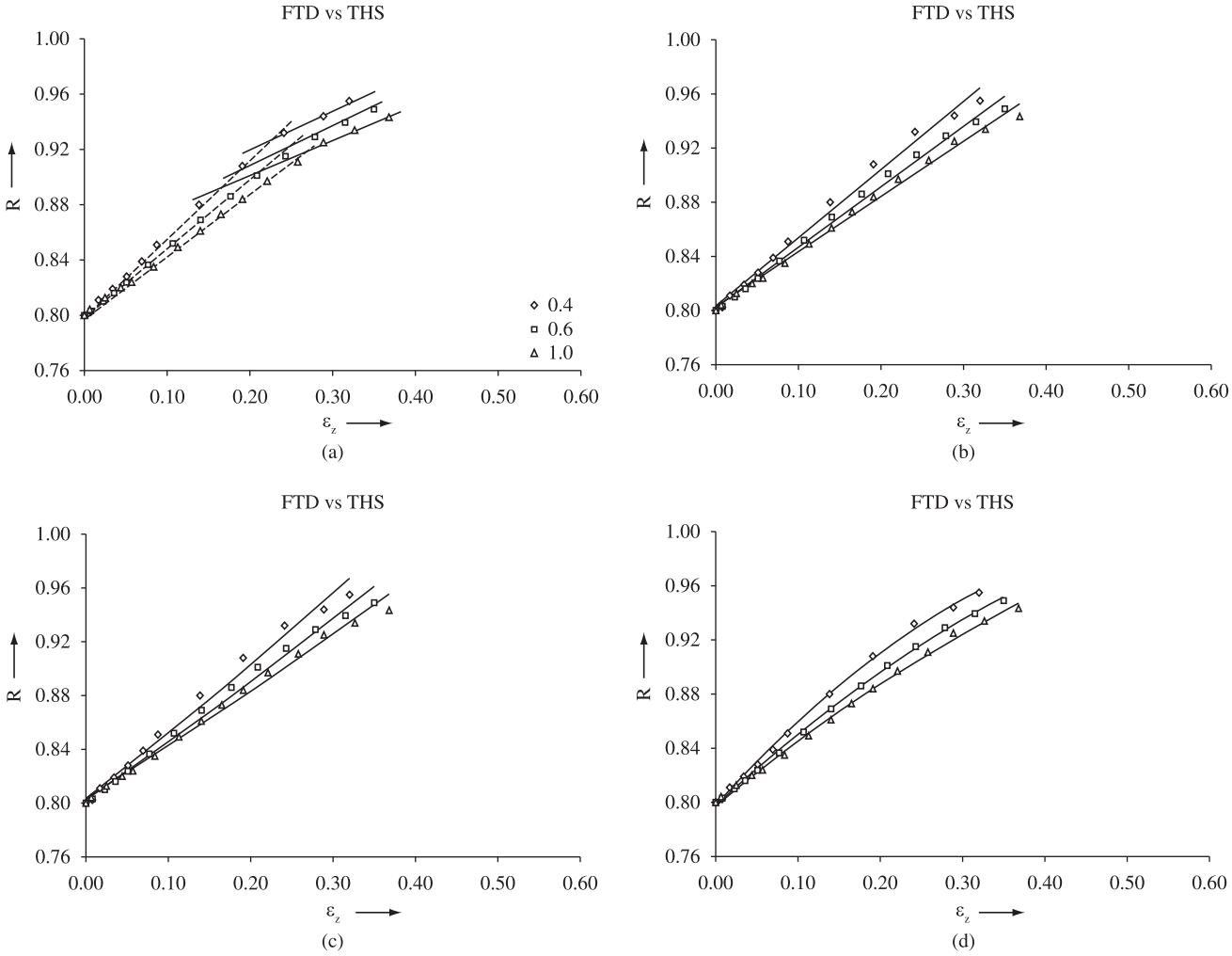

Figure 3. a) Relationship between R and ε_z; b) relationship between R and ε_z – linear curve fitting; c) relationship between R and ε_z – exponential curve fitting; and d) relationship between R and ε_z – parabolic curve fitting.

Table 2. Curve fitted results between R and ε_z.

Relationship	Aspect ratio	Name of the curve	Empirical equation	RC value
R vs. ε_z	0.40	Linear	$R = 0.5035\varepsilon_z + 0.8035$	0.9907
	0.60		$R = 0.4464\varepsilon_z + 0.8022$	0.9939
	1.0		$R = 0.4077\varepsilon_z + 0.8027$	0.9946
	0.40	Exponential	$R = 0.8047e^{0.575\varepsilon z}$	0.9869
	0.60		$R = 0.8034e^{0.51226\varepsilon z}$	0.9906
	1.0		$R = 0.8040e^{0.4689\varepsilon z}$	0.9921
	0.40	Polynomial	$R = -0.5635\varepsilon^2_z + 0.6765\varepsilon_z + 0.7974$	0.9985
	0.60		$R = -0.3537\varepsilon^2_z + 0.5632\varepsilon_z + 0.7974$	0.9991
	1.0		$R = -0.2325\varepsilon^2_z + 0.4879\varepsilon_z + 0.7990$	0.9979

every value of aspect ratio, however lower initial aspect ratio exhibited improved density at any given level of strain. The aforementioned phenomena can be grasped from Figure 3a, as it shows the general characteristic behavior which shows two different stages of densification with respect to induced axial strain, respectively shown by dotted and continuous line. While Figure 3b, c demonstrates various curve fitting techniques adopted for the aforementioned relationship, on which parabolic curve or polynomial of second order found to be the best for the selected ranges of aspect ratios. The corresponding empirical relations and its regression coefficient value been given in Table 2. Thus, parabolic curve found to the best fit, which is chosen for the explanation of densification mechanism with respect to axial strain along with Figure 3a, as it explores the stages of densification during deformation.

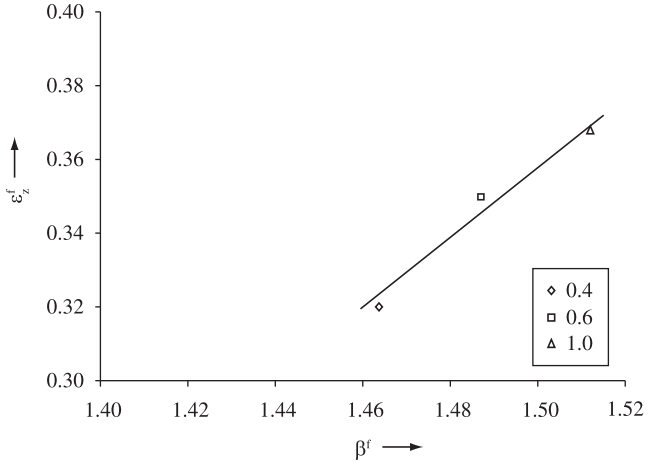

Figure 4. Relationship between ε_z^f and β^f.

For instance, when there is no axial strain then the value of *R* in polynomial expression is just constant, which is found to be the initial relative density of the preform that is kept as constant of value 80%. However, this constant only indicates the starting point of the densification curve and can change if the initial preform density is changed, accordingly, it is anticipated that other constants will also be highly influenced and hence the overall densification behaviour. The values corresponding to 'ε_z' term in polynomial equations are positive irrespective of the aspect ratios. Hence, it is taken for granted that this parameter conclusively contributes to densification and enhances the same linearly as it is multiplied directly by the axial strain. However, the constant corresponding to 'ε_z^2' term has been observed to be negative and also is multiplied by the square of the bulging ratio and hence its contribution is negative to densification. In fact, this

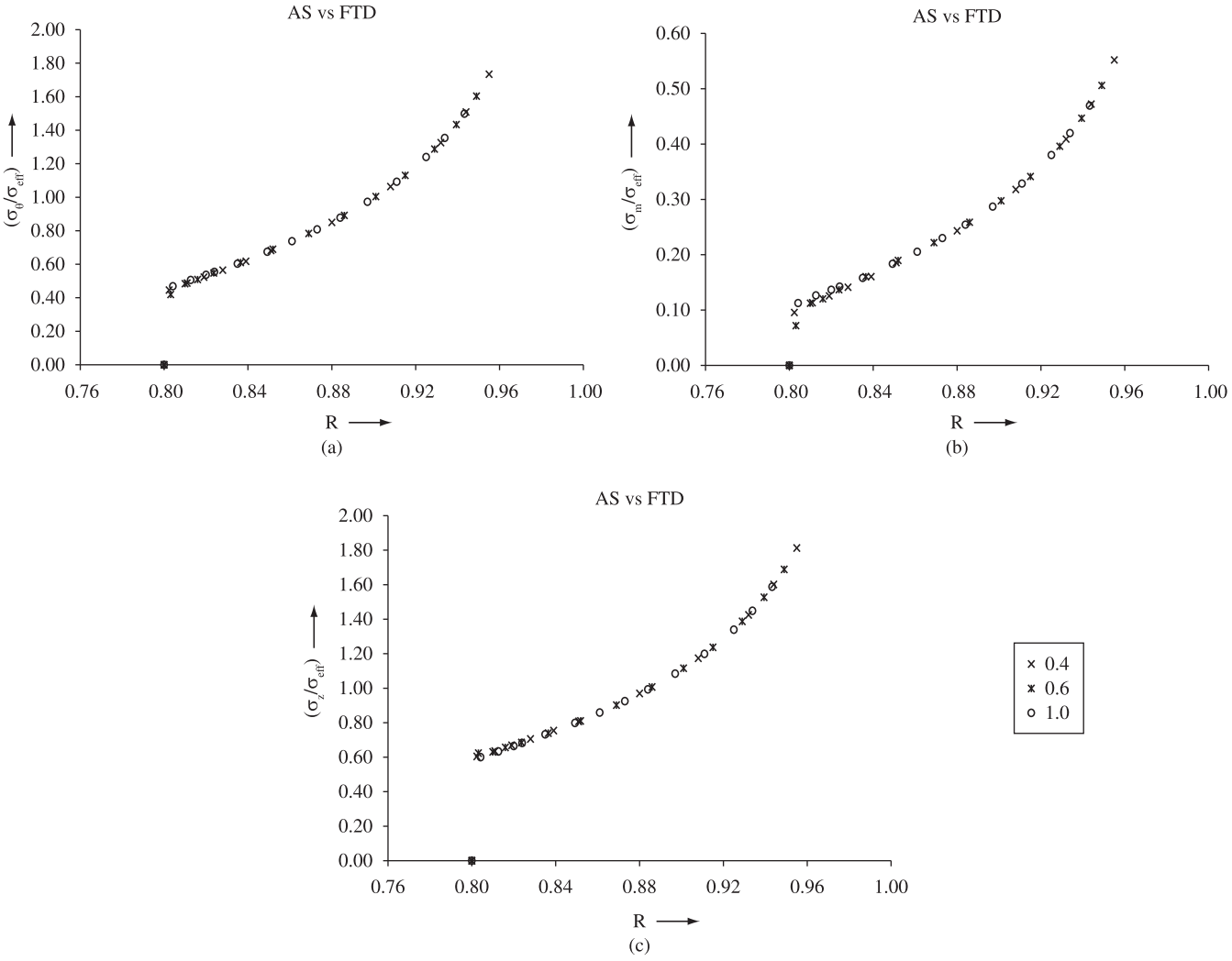

Figure 5. a) Relationship between (σ_0/σ_{eff}) and *R*; b) relationship between (σ_m/σ_{eff}) and *R;* and c) relationship between (σ_z/σ_{eff}) and *R*.

contributes to plateau the curves in the final stages of densification when the value of axial strain starts exceeding approximately 0.25.

Upsetting has been carried out till preform experience crack at the free surfaces and that was carefully noted, as these data leads to more flexibility for designers and better optimization of parts, particularly in the design of the preform shape and dies. Indeed, if the preform forged in a confined die, the process will undergo two different stages. This is upsetting or compression with free lateral flow followed by contact of the metal flow with die walls, which redistributed the lateral flow in repressing mode of deformation. Thus, the preform shape must be determined such that the part should be produced with fracture free surface since there is little possibility that the cracks can be arrested during the repressing stage of deformation. Therefore, the experimental data obtained during cold upsetting mode of deformation for Cu-7%Al-1.8%Si has been utilized to establish relationship between the axial strain at fracture (ε_z^f) and stress formability index at fracture (β^f) for all the selected initial aspect ratio as shown in Figure 4.

It can be observed that the increase in height strain at fracture with the increasing initial aspect ratio of the preforms. This is due to the fact that higher the aspect ratio possess higher the volume of material which eventually has higher the pore bed, thus the transformation of deformation between particles consume more energy that eventually takes more strain to fracture. A straight line fitting is used for this plot and the slope of it is found to be 0.97. This plot could be effectively utilized to the design of preforms, such as selection of preform geometry (initial aspect ratio). In addition to this, the appropriate introduction of die constraint at the free surface of deforming preform can be evaluated.

Figures 5a through c is drawn for hoop ($\sigma_\theta/\sigma_{eff}$), mean ($\sigma_m/\sigma_{eff}$) and axial ($\sigma_z/\sigma_{eff}$) stress ratios to that of relative density (R) respectively for the copper alloy of various aspect ratios under cold upsetting of triaxial stress state condition.

The general stress ratio behaviour of the preform against the attained density was found to be identical. Further it is interesting to note that variation of aspect ratios made zero impact on the stress ratio behaviour. However, the highest stress ratio value obtained for the smallest aspect ratio, which is true for all the stress ratio conditions. Also it is found that the increasing aspect ratio decreases the magnitude of highest stress ratio, which indicates that higher aspect ratio preforms has further chance to deform, provided preform is not fractured. In otherwise, lowering the aspect ratios effectively lowers the volume of the materials which promotes enhanced deformation and densification subsequently promoting strength in it comparing to the higher aspect ratio preforms before it fractures.

5. Conclusions

Workability analysis of sintered copper alloy of various aspect ratios revealed the critic metrics such as the parabolic curve to be found as best fit in expressing the behavior of stress formability index and obtained density against induced axial strain. Decreasing the aspect ratio facilitates uniform deformation results into enhancement in densification and stress formability index for any given value of strain, however limits the height strain to facture. Further it is to be concluded that variation of aspect ratios made nil impact on the various stress ratio behavior against densification.

References

1. Saanouni K. On the numerical prediction of the ductile fracture in metal forming. *Engineering Fracture Mechanics*. 2008; 75(11):3545-3559.
2. Venugopal Rao A, Ramakrishnan N and Krishna Kumar R. A comparative evaluation of the theoretical failure criteria for workability in cold forging. *Journal of Materials Processing Technology*. 2003; 142(1):29-42.
3. Landre J, Pertence A, Cetlin PR, Rodrigues JMC and Martins PAF. On the utilization of ductile fracture criteria in cold forging. *Finite Element in Analysis and Design*. 2003; 39(3):175-186.
4. Petruska J and Janicek L. Computationally-Experimental Workability Determination of Compressed Cylindrical Specimen with Surface Defects. *Journal of Materials Processing Technology*. 1998; 80-81:572-578.
5. Abdel Rahman M and El-Sheikh. Workability in Forging of Powder Metallurgy Compacts, *Journal of Materials Processing Technology*. 1995; 54:97-102.
6. Hoa VC, Seo DW and Lim JK. Site of ductile fracture initiation in cold forging: a finite element model. *Theoretical and Applied Fracture Mechanics*. 2005; 44(1):58-69.
7. Tahir SM and Ariffin AK. Fracture in Metal Powder Compaction. *International Journal of Solids and Structures*. 2006; 43(6):1528-1542.
8. Cheng NP, Zeng SM and Liu ZY. Preparation, Microstructures and Deformation Behavior of SiCp/6066Al Composites Produced by PM Route. *Journal of Materials Processing Technology*. 2008; 202(1-3):27-40.
9. Vujovic V and Shabaik AH. A New Workability Criterion for Ductile Materials. *Journal of Engineering Materials and Technology, ASME*. 1986: 108:245-249.
10. Wifi AS, Abdel-Hamid A and El-Abbasi N. Computer Aided Evaluation of Workability in Bulk Forming Processes. *Journal of Materials Processing Technology*. 1998; 77(1-3):285-293.
11. Lin Hua, Xunpeng Qin, Huajie Mao and Yumin Zhao. Plastic Yield Deformation and Yield Criterion for Compressible Sintered Powder Materials. *Journal of Materials Processing Technology*. 2006; 180(1-3):174-178.
12. Pokorska. Experimental Identification of Yield Stress for Sintered Materials. *Powder Metallurgy and Metal Ceramics*. 2008; 47(7-8):393-397.
13. Notych AA. Determination of the Stress-Strain State when Examining the Limiting Plasticity of Porous Parts. *Powder Metallurgy and Metal Ceramics*. 1998; 37(5-6):244-248.
14. Aubertin M and Li Li. A Porosity Dependent Inelastic Criterion for Engineering Materials. *International Journal of Plasticity*. 2004; 20(12):2179-2208.
15. Amosov AP and Fedotov AF. Variant of Plasticity Condition for Powdered Solids. *Powder Metallurgy and Metal Ceramics*. 2000; 39(3-4):116-121.
16. Justino JG, Alves MK, Klein AN and Al-Qureshi HA. constitutive model for the elastic-plastic analysis of porous sintered materials. *International Journal of Machine Tools and Manufacture*. 2004; 44(14):1471-1479.
17. Justino JG, Alves MK, Klein AN and Al-Qureshi HA. A comparative analysis of elasto-plastic constitutive models for porous sintered materials. *Journal of Materials Processing Technology*. 2006; 179(1-3):44-49.
18. Narayanasamy R and Pandey KS. Salient Features in the Cold Upset-Forming of Sintered Aluminium-3.5% Alumina Powder Composite Preforms. *Journal of Materials Processing Technology*. 1997; 72(2):201-207.
19. Narayanasamy R and Pandey KS. A Study of Barreling Aspects on P/M Iron Preforms during Hot Upset Forming. *Journal of Materials Processing Technology*. 2000; 100:87-94.
20. Doraivelu SM, Gegel HL, Gunasekara JS, Malas JC, Morgan JT and Thomas Jr JF. New Yield Function for Compressible P/M Materials. *International Journal of Mechanical Sciences*. 1984; 26(9-10):527-535.
21. Rajeshkannan A, Pandey KS and Shanmugam S. Some Investigation on the Cold Deformation Behaviour of Sintered Iron–0.8% Carbon Alloy Powder Preforms. *Journal of Materials Processing Technology*. 2008; 203:542-547.

Appendix 1. Notation.

Notation	
0.4, 0.6 & 1.0	Aspect ratio (height to diameter ratio)
σ_z	Axial stress
σ_{eff}	Effective stress
σ_r	Radial stress
σ_θ	Hoop stress
σ_m	Mean stress
ε_θ	Hoop strain
ε_r	Radial strain
ε_{eff}	Effective strain
ε_z	Axial strain
ε_z^f	Axial strain to fracture
β	Stress formability index
β^f	Stress formability index at fracture
H_o	Initial height of preform
H_f	Height of preform after deformation
D_o	Initial diameter of preform
D_f	Contact diameter after deformation
D_b	Bulged diameter after deformation
ϕ_{eff}	Forming limit strain
$d\varepsilon_\theta$	Plastic hoop strain increment
$d\varepsilon_z$	Plastic axial strain increment
γ	Poisson's ratio
R	Relative density